

## Experimental investigation of masonry walls supported by steel plate-masonry composite beams

Deng-Hu Jing<sup>\*1</sup>, Jian-Fei Chen<sup>2</sup>, Giuseppina Amato<sup>2</sup>, Ting Wu<sup>1</sup> and Shuang-Yin Cao<sup>1</sup>

<sup>1</sup> School of Civil Engineering, Southeast University, Nanjing, Jiangsu, 211189, China

<sup>2</sup> School of Natural and Built Environment, Queen's University Belfast, Belfast BT9 5AG, UK

(Received October 2, 2017, Revised April 8, 2018, Accepted July 15, 2018)

**Abstract.** Masonry walls are sometimes removed in buildings to either make new passages or increase the usable space. This may change the loading paths in the structure, and require new beams to transfer the loads which are carried by the masonry walls that are to be removed. One possible method of creating such new beams is to attach steel plates onto part of the existing walls to form a steel plate-masonry composite (SPMC) beam, leading to a new structure with part of the masonry wall supported by a new SPMC beam. This paper presents an experimental investigation into the interaction between the SPMC beam and the masonry wall above. Five SPMC beams supporting a masonry wall were tested to study the influence of parameters including the height-to-span ratio of the masonry wall, height of the beam and thickness of the steel plates. The test results, including failure mode, load-carrying capacity, load-deflection curves and strain distribution, are presented and discussed. It is found that for developing better arching effect in the masonry wall the ratio of the in-plane flexural stiffness of the masonry wall to the flexural stiffness of the SPMC beam must be between 2.8 and 7.1.

**Keywords:** steel plate-masonry composite (SPMC) beam; masonry wall; arching effect; flexural stiffness; local buckling

### 1. Introduction

A significant part of the building stock built before 1980s in China is masonry structures. Many of them need strengthening for either improving their static load-carrying capacity or seismic performance, or renovation of the building. In recent years, strengthening of unreinforced masonry structures has received more and more attention of civil engineers and researchers across the world (Taghdi *et al.* 2000, Konthesingha *et al.* 2013, Farooq *et al.* 2014a, b, El-Diasity *et al.* 2015, Ismail *et al.* 2015, Santis *et al.* 2016, 2018, Martinelli *et al.* 2016, Guerreiro *et al.* 2018, Kariou *et al.* 2018, Preciado *et al.* 2018, Wang *et al.* 2018). However, masonry walls are sometimes removed in existing buildings to alter their functions, e.g., to create new passages or increase usable spaces. Such changes alter the loading paths in the structure, and require the installation of new beams to transfer the loading away from the new openings. Traditionally, new reinforced concrete (RC) or steel beams are installed for this purpose (Jing 2017, Hardy 2000). An alternative technique for creating such new load bearing elements is to attach steel plates onto a part of the existing wall through bolts and bonding to form a steel plate-masonry composite (SPMC) beam for supporting the masonry wall above. This technique has some competitive advantages over conventional RC beams, including reduced wet work, avoidance of formwork, time saving, ease of

installation and minimal increase of dimensions. The technique has been used in a number of projects in China (Jing 2017). Fig. 1 shows a building during and after renovation in Nanjing, where the ground floor was opened as parking spaces.

A series of tests have been conducted at Southeast University to study the behavior of SPMC beams and SPMC columns under monotonic loading (Jing *et al.* 2011, 2012 and 2013), and SPMC moment-resisting frames under low frequency reversed cyclic loading (Jing 2017). The effects of the main parameters have been investigated, including the injection materials (cement grout and epoxy adhesive), the thickness of steel plates and the spacing of bolts which pass through the beam or column width to connect the two steel plates on the two opposite faces (Jing *et al.* 2012, 2013, Jing 2017). The results of these studies showed that SPMC beams and columns can be designed to have sufficient load-carrying capacity and stiffness for common use in building renovations, and SPMC frames have good ductility and energy dissipation capacity. SPMC beams with a span of up to 8.5 m have been used in practice (Jing 2017).

When a beam is introduced to create an opening in an existing building it will interact with the masonry wall above, forming a composite wall-beam structure. This interaction has been studied between both RC (Hossain *et al.* 2000) and steel beams and the supported masonry walls subjected to a uniformly distributed loading on the wall (Soltis and Tuan 1980, Smith *et al.* 1982, Hardy and Al-Salka 1995, Hardy 2000, Borri *et al.* 2009). However, to the best knowledge of the authors, no studies have been

\*Corresponding author, Ph.D., Associate Professor,  
E-mail: [jingdh@seu.edu.cn](mailto:jingdh@seu.edu.cn)



(a) During construction work

(b) After construction work

Fig. 1 A renovation project in Nanjing using SPMC beams

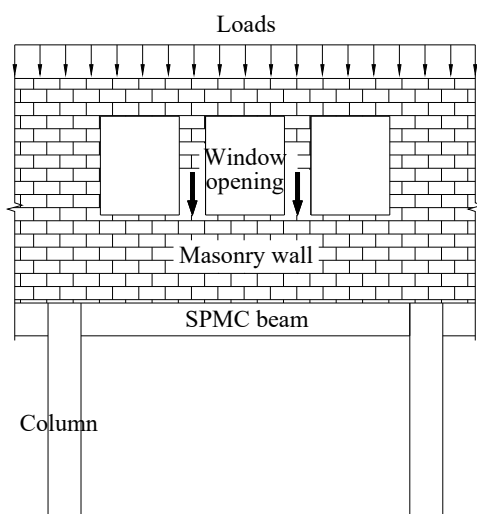


Fig. 2 Typical loading schemes on SPMC beam-wall

reported in the literature on the interaction between masonry walls and SPMC beams.

Although the most common loading on the masonry wall above an SPMC beam may be a distributed load, the load is not necessary a uniformly distributed. When there are window openings above the wall the loading may be modelled as a set of concentrated forces acting between the window openings at the window sill level (see Fig. 2). This study thus focuses on the SPMC beam-walls under concentrated loads.

## 2. Experimental program

### 2.1 Test specimens

In this study five SPMC beam-wall specimens (B1-B5) were designed and tested under two point loads (four point bending test) to simulate the load distribution shown in Fig. 2. The *SPMC beam* designates the part of the masonry wall encased by the steel plates, the *wall* the remaining masonry wall after the removal of the lower parts, and *SPMC beam-wall* the overall ensemble. The influence of the height-to-span ratio of the masonry wall above the SPMC beam, the height of the SPMC beam and the thickness of the steel plates were considered as research variables, see Table 1.

The SPMC beams consisted of a masonry beam with steel plates on the side and bottom face. The specimens had a gross span of 2200 mm, with a clear span ( $l_0$ ) of 2000 mm between the two supports. The three steel plates with pre-drilled holes were welded along the edges, forming a channel section and the 240 mm thick clay brick masonry was then laid on it. A 10 mm clear gap between the vertical faces of the steel channel and the masonry was later filled with cement grout. Holes in the masonry were drilled through the pre-drilled holes in the steel plates for the installation of bolts for restraining the plates on the two faces of the masonry wall. All the bolts were 14 mm diameter threaded steel rods. Based on common practice and on previous experimental results obtained by the authors (Jing *et al.* 2012) a bolt spacing of 250 mm was used to ensure that the steel-encased-masonry behaved as a

Table 1 Geometrical data of specimens

Specimen	Beam width $w_b$ (mm)	Beam height $h_b$ (mm)	Wall height $h_w$ (mm)	$h_w/l_0$	$h_b/l_0$	Thickness of bottom steel plate $t_1$ (mm)	Thickness of side steel plates $t_2$ (mm)
L2	240	355	/	/	0.178	5.6	5.6
B1	240	350	500	0.25	0.175	5.5	5.5
B2	240	350	800	0.40	0.175	5.5	5.5
B3	240	350	1100	0.55	0.175	5.5	5.5
B4	240	350	800	0.40	0.175	7.9	9.4
B5	240	550	800	0.40	0.275	5.5	5.5

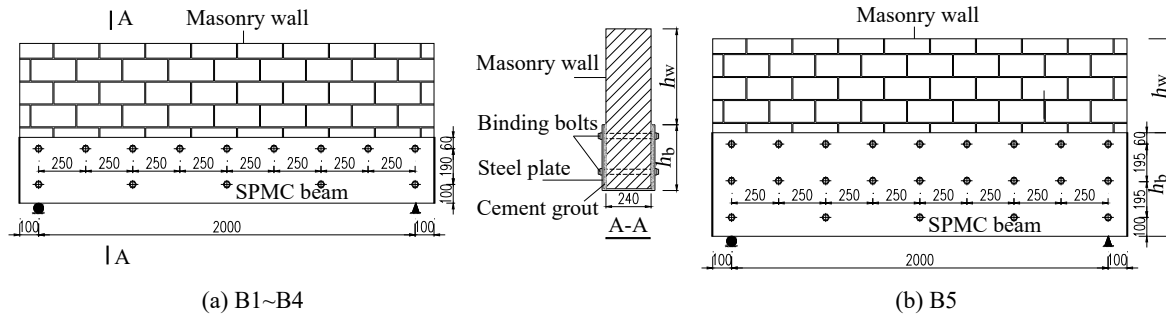


Fig. 3 SPMC beam-wall specimens

composite steel-masonry beam. This spacing gave a maximum ratio of the bolt spacing to the thickness of steel plate equal to 45.5. Details of the specimens are shown in Fig. 3.

For ease of comparison the SPMC beam of specimen B1 was designed to have the same geometry of specimen L2 reported in Jing *et al.* (2012) where the SPMC beam L2 had no masonry wall above and was tested under the same loading scheme as in this study.

Portland cement 32.5 was used for the cement grout which had a water/cement ratio of 0.6. A small amount of water was added (increasing the W/C ratio to up to 0.8) at places where the grout was too dry to fill. The mechanical properties of the steel plates, bolts, masonry, and cement grout were determined following the relevant Chinese standards. The thicknesses of the steel plates were 5.5, 7.9 and 9.4 mm. The mechanical properties of the steel plate, binding bolt, and encased masonry were determined using three samples for each type of steel plate, three samples for the steel rod, and six samples for the masonry (GB/T 228.1-2010 2010, GB/T 50129-2011 2011). The average values of the test data are reported in Table 2.

2.2 Test setup and instrumentation

The specimens were tested under two point loads. The distance between the two point loads was 700 mm, leaving a shear span of 650 mm on each side. The load was applied with a 3200 kN hydraulic jack through a steel loading beam as shown in Fig. 4.

The specimens were instrumented to measure the

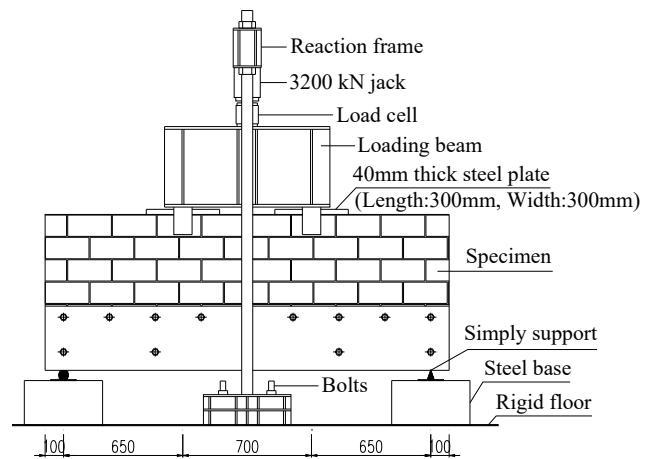
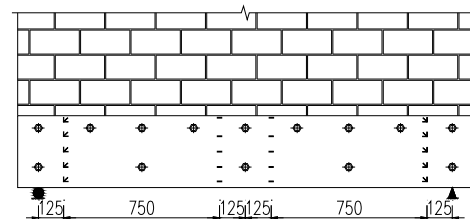
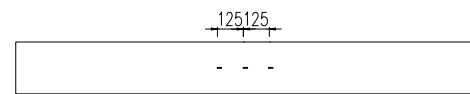


Fig. 4 Test setup



(a) Side steel plates



(b) Bottom steel plate

↙ Strain rosette    -    Strain gauge

Fig. 5 Layout of strain gauges

Table 2 Material properties

Element	Thickness/ diameter (mm)	Yield strength (MPa)	Ultimate strength (MPa)	Elastic modulus (MPa)
Steel plates	5.5	354.3	490.0	200000
	7.9	343.0	450.0	200000
	9.4	326.6	483.5	200000
Bolts	14	401.6	526.1	210000
Element	Compressive strength (MPa)			
Masonry	8.20			
Cement grout	15.5			

midspan displacement with a linear variable differential transformer (LVDT) at the midspan, and two dial indicators at both supports to record settlements. Strain gauges were bonded on the steel plates to monitor strain development. Twenty strain gauges in four rows were installed on each side of the steel plates at 125 mm from the mid span and from the two supports (see Fig. 5(a)). Three strain gauges were also installed on the bottom plate (see Fig. 5(b)). Both strains and displacements were recorded using a data logger (Data Taker DH3815) and the applied load was recorded using a load cell.

### 2.3 Test procedure

The specimens were tested monotonically until failure. A finite element analysis was carried out prior to the testing to estimate the failure load. All specimens were pre-loaded to about 5% of the predicted failure load to ensure that the instrumentation was working properly and there was no slack in the system. The preload was then released and the readings were set to zero. The loading test was carried out in force control by increments of about 5% of the failure load ( $\sim 20$  kN). The specimen after each loading increment was left to rest for 3 minutes before readings were recorded.

## 3. Test results and discussion

### 3.1 Failure modes

Specimen B1 failed in diagonal-tension. A crack of about 38-degree to the horizontal initiated along the mortar-brick interfaces at about midpoint between the loading point and the left support (see Fig. 6(a)). It propagated quickly at both sides and reached the support at the left and loading position at the right, well before final failure. The ultimate state was reached when the diagonal crack widened so much that the triangular block of masonry on the left side was completely detached. The side steel plates in the SPMC beam experienced local buckling shortly after the crack appeared in the masonry (see Figs. 6(b) and 7). This indicates that the top part of the plates experienced high compressive stresses. The masonry wall had a height-to-span ratio of 0.25 in this specimen.

Cracking in specimen B2 started similarly than in specimen B1, but due to the large height-to-span ratio of B2



(a) Crack in the masonry wall



(b) Local buckling of the steel plate (view from above)

Fig. 6 Specimen B1 at failure

(0.40), the masonry wall experienced a shear-compression failure with diagonal cracks at 55-60 degrees to the horizontal (Fig. 8). The side steel plates buckled locally before the ultimate state was reached.

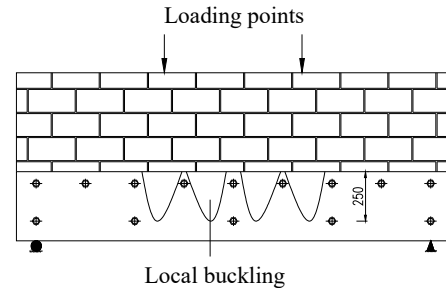


Fig. 7 Local buckling of steel plates in specimen B1



Fig. 8 Cracks in the masonry wall in specimen B2



Fig. 9 Cracks in the masonry wall of specimen B3



Fig. 10 Specimen B4 at the end of test

Specimen B3 had an even larger height-to-span ratio of 0.55 for the masonry wall. Splitting-tension shear cracks were developed in the masonry wall (see Fig. 9) above the supports at about 200 mm above the SPMC beam and then propagated towards the loading points. A brittle failure followed closely the cracking load. The side steel plates did not show any visible local buckling.

Specimen B4 had the same masonry height-to-span ratio as in specimen B2, but thicker steel plates (see Table 1). The failure mode was very similar to that of specimen B2 (see Fig. 10).

Specimen B5 also had a masonry height-to-span ratio of 0.40 as specimen B2, but had a higher SPMC beam (see Table 1). The first crack initiated along the mortar-brick interfaces between the loading point and the support and propagated diagonally through the bricks as the load increased. Following the development of the above cracks,

a nearly vertical crack also occurred under the loading point (Fig. 11(a)), and small local buckling occurred in the steel plates near the midspan. When the vertical crack extended downwards at about 60% of the failure load, a small amount of the masonry under the loading point was crushed and part of it spalled, while another diagonal crack nearer the support was formed. The ultimate state was reached when a large block of the wall was detached (Fig. 11(b)). Note that the flexural stiffness of the SPMC beam was the largest among the five specimens. Under the same vertical loading, it thus had the smallest deflection leading to more evenly distributed beam-wall contact stresses. A mixed failure mode developed: a diagonal-tension failure mode and a shear-compression failure mode with several approximately vertical local compression cracks accompanied by local crushing and spalling (Fig. 11(b)).

### 3.2 Load-deflection behavior

Fig. 12 shows the load-deflection curves of the specimens. The cracking load and local buckling load are indicated on the plots.

The curves are generally irregular with several small changes of stiffness, both positive and negative before the cracking load is reached. Specimen B2 has an initial smoother trend that makes exception to this tendency.

Specimen B3 experienced a premature failure just after cracking. Except for this specimen, a clear inverse proportional trend between maximum deflection and maximum capacity can be seen. Specimen B1 had the largest deflection (11.22 mm), almost the double of Specimen B2 (6.44 mm) which had the same SPMC beam height but a higher masonry wall. Among specimens B2, B4 and B5 (same wall height but increasing beam stiffness), specimen B5 showed the highest failure load and the smallest deflection (3.96 mm).

The slope of the first branch of the curves increased with the wall height for specimens B1 and B2 (having the same beam geometry) but not for B3. The initial slope also increased, as expected, as the beam stiffness increased (B2, B4 and B5).

### 3.3 Midspan strain distribution in steel plates

Figs. 13(a)-(e) shows the strain distribution at midspan along the depth of the steel plates for increment of loads of about 20% of the failure load. Note that each point represents the average of four strain readings at the same height (two on each face). The development of average compression strain at the top edge of the side plates (10 mm away from the top) near the midspan is illustrated in Fig. 14.

As shown by Fig. 13 the bottom plate yielded in specimen B1 and approached yielding in specimen B2, but it did not yield in other specimens. The strain distributions in the steel plates are close to the plane section assumption, but the bottom strain has some deviation probably due to the unequal distribution of the bolts.

For specimens with same SPMC beam but different masonry wall heights (B1, B2 and B3) the depth of the neutral axis from the bottom face increased with the wall



(a) Cracks during the test



(b) Final failure mode

Fig. 11 Specimen B5

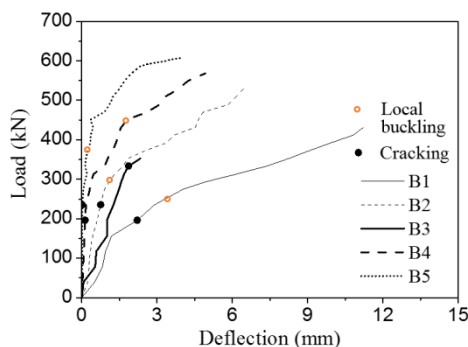


Fig. 12 Load-deflection curves

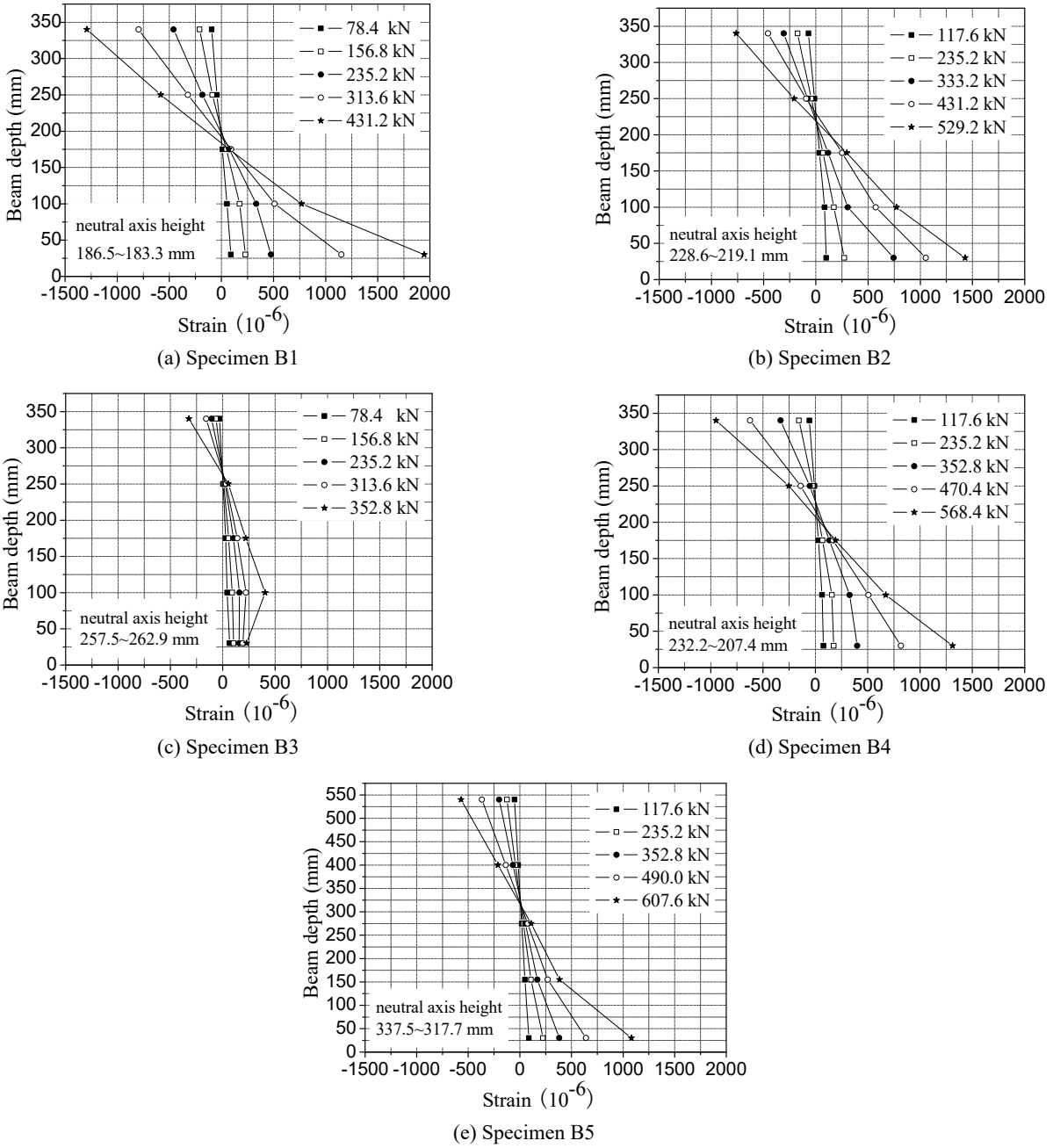


Fig. 13 Strain distribution across the depth of steel plate section

height from about 180 mm to 260 mm (from 0.51 to 0.74 of the beam total depth), see Figs. 13(a)-(b)-(c). This trend hints that the higher wall specimens developed an arching actions and this induced the SPMC beam to act as a tie. This is also confirmed by the lower values and slowest development of compression strains, for same level of load in specimens B2, B3 compared to B1 (Fig. 14), as in these specimens the compression stress due to bending moment was counteracted by the tensile stress due to the arching thrust of the wall.

Looking at specimens B2, B4 and B5 with same wall height and different beam stiffness, one can note that B2 and B4 had a similar response (same neutral axis depth and load-strain curves, see Figs. 13(b), (d) and 14). These two specimens differed only for the steel plate thickness. Based

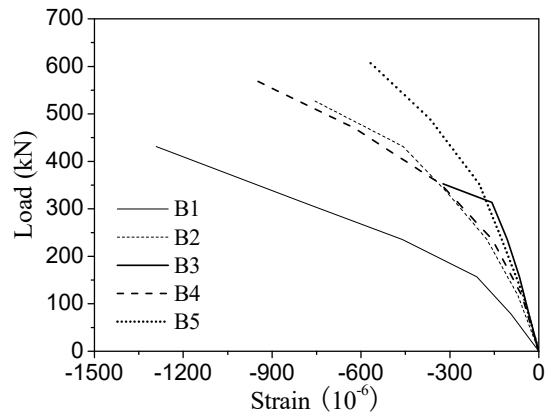


Fig. 14 Load versus compression strain at the top edge

on these experimental results, the beam-wall interaction was not affected by the small difference of beam stiffness. In specimen B5 the neutral axis depth was lower than the one in B2 (0.58 vs 0.63 of beam depth). This was expected due to the high beam stiffness and more evenly distributed beam-wall contact stresses. On the other side the strain values for same level of load are much smaller than in specimen B2 but this is to be expected due to the higher moment of inertia of the beam in B5.

### 3.4 Stress in the steel plates near the supports

As shown in Fig. 5, multi-axial strain gauges (rosettes) were set to monitor the stress development of the steel plates near the supports. Based on the measured data, the maximum equivalent von Mises stresses of steel plates for specimens B1 to B5 are 174.3 MPa, 202.0 MPa, 140.3 MPa, 173.9 MPa and 243.0 MPa, respectively. The ratios of the calculated maximum equivalent von Mises stress to the yielding stress are 49%, 57%, 40%, 53%, and 69%, respectively indicating that the steel plate did not yield at failure. Also, local buckling near the supports did not take place.

Fig. 15 presents the evolution of principle stresses angle (average value of midpoint of the beam) at the rosette near the supports. The angle decreases as the load increases from maximum values of about 65 degrees to minimum values of about 30 degrees. In the middle and late state of loading, the angle of specimens B2, B3 and B4 was significantly larger

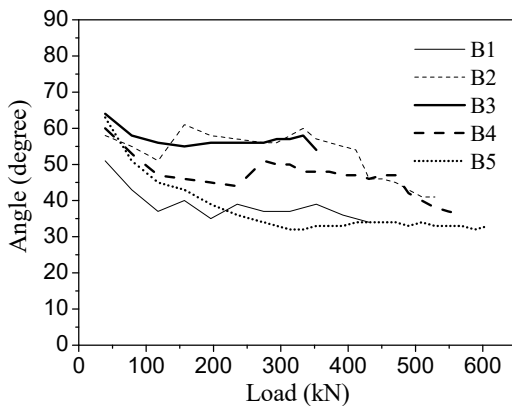


Fig. 15 Angle of principle compressive stresses to the horizontal axis

than that of specimens B1 and B5; the former angles were about 45~55 degrees, and the latter angles were about 30~40 degrees.

### 3.5 Local buckling of the steel plates

The load at which the steel plates experienced local buckling has been reported in Table 3. The local buckling load is an important parameter for practical design because local buckling in service is undesirable, although there is usually a significant post-buckling strength reserve. In Jing *et al.* (2012) the local buckling load was detected as the state of local separation between a steel plate and the encased masonry. For the specimens in this study the local buckling phenomena were identified by eye observation and knocking on the surface of steel plates to identify their separation from the masonry wall.

Specimens B1-B5 had higher buckling load than specimen L2 (SPMC beam with no wall). However, it should be noted that the bolt spacing was 300 mm in L2 and 250 mm in the present study specimens. Specimens L2, B1, B2 and B3 had the same SPMC beam geometry but increasing wall height ( $h_w/l_0$  values between 0 and 0.55), showed increased levels of the buckling load (from 15% to > 77% compared to B1). This could be attributed a lower compressive stress at the top of the steel plates for the same level of external load.

Compared to specimen B2, the local buckling load of specimen B4 having thicker side steel plates (5.5 mm versus 9.4 mm respectively, an increase of 64% of the cross-sectional area of steel plates) increased by 53%. However, the failure load of B4 increased by only 7% with respect to

Table 4 Comparison of wall-beam stiffness ratios

Specimen	Wall height-to-span ratio	Wall/SPMC beam stiffness ratio	Arching action	Failure load
	$h_w/l_0$	$R$		
B1	0.25	0.91	No	431.2 kN
B2	0.40	3.72	Yes	529.2 kN
B3	0.55	9.68	Yes	352.8 kN
B4	0.40	2.76	Yes	568.4 kN
B5	0.40	1.07	Very weak	607.6 kN

Table 3 Loading capacities

SPMC beam	Cracking load (kN)	Local buckling load (kN)	Failure load (kN)	Compared to B1		Compared to L2	
				Local buckling load ratio	Failure load ratio	Local buckling load ratio	Failure load ratio
L2	/	238.5	356.0	/	/	/	/
B1	196.0	255.0	431.2	/	/	1.07	1.21
B2	235.2	294.0	529.2	1.15	1.23	1.23	1.49
B3	333.2	/	352.8	>1.38	0.82	>1.48	0.99
B4	196.0	450.8	568.4	1.77	1.32	1.89	1.60
B5	235.2	372.4	607.6	1.46	1.41	1.56	1.71

B2 as the ultimate state of SPMC beam-wall was controlled by the failure of the wall rather than the SPMC beam. The local buckling load of specimen B5 was 27% higher than B2 (which had the same wall height) because specimen B5 had a deeper SPMC beam resulting in lower compression stresses.

### 3.6 Load-carrying capacities

In Table 3 the cracking and ultimate failure loads for specimens B1-B5 are reported. The results for SPMC beam L2 from Jing *et al.* (2012) are also reported for comparison purpose. Specimen B1 having a 500 mm high masonry wall above the SPMC beam increased the failure load capacity by about 20% compared to specimen L2. It should be noted that the steel plates in specimen L2 had yield strength of 308.7 MPa, 9.6% lower than the average yield strength of the steel in this study, so the actual contribution of the 500 mm wall to the loading capacity in specimen B1 should be less than 20%. The failure loads of specimen B2, B4 and B5 are significantly higher than specimen B1. This can be attributed to the different failure mode of masonry wall that determined the ultimate state, i.e., compressive strength greater than shear strength and minimum tensile strength. In this type of wall-beam structural elements, the masonry failure model is controlled by the beam stiffness relative to the masonry wall.

Specimen B3 had the highest wall yet the lowest failure load, because the splitting-tension cracks in the masonry above the support caused a premature failure of the wall. It implies that for SPMC beam-walls, a moderate wall height is crucial to develop an optimal interaction between the SPMC beam and the supported masonry wall.

## 4. Discussion and recommendations

Test results obtained in this study show that to generate arching action in the masonry wall and develop better interaction between the masonry wall and the SPMC beam, a minimum value of height-to-span ratio of the masonry wall is needed. A comparison between specimen B1 and SPMC beam only specimen L2 tested by Jing *et al.* (2012) shows that the local buckling and failure load of specimen B1 are 7% and 21% respectively higher than specimen L2. However, since specimen L2 has also a lower steel yielding value (-9.6%), specimen B1 behaves almost like specimen L2, that is as an ordinary flexure-dominated SPMC beam. This is further proved by the fact that the bottom plate and near-bottom side plate in specimen B1 yielded and the steel plates in the compression zone, unlike other specimens, exhibited clear local buckling. Therefore, a wall height-to-span ratio higher than 0.25 is required to develop interaction between the masonry wall and the SPMC beam.

Specimens B2, B4, with a height-to-span ratio of the masonry wall of 0.4, had local buckling and failure loads significantly increased in comparison to B1, indicating that arch effect occurred in the masonry walls. In fact, when the masonry wall exhibits arch effect, the SPMC beams work as a beam under combined bending (due to the vertical load) and tension (induced by the thrust of the main arch). This

explains why in these specimens the neutral axis height of the beam moved upward and the side plates experienced light local buckling. As a conclusion, the beam-wall interaction takes place for SPMC wall-beam with wall height-to-span ratio of 0.4.

Fig. 13 shows that the steel plate of the SPMC beam in specimen B3 had a very small strain even at the ultimate state, and did not experienced any local buckling. Furthermore, assuming a local buckling load at least equal to the failure load, specimen B3 showed an increase of at least 48% compared to specimen L2. From these results the wall-beam interaction in specimen B3 was significant, but the higher masonry height determined a splitting-tension failure and a markedly low failure load compared to B2 or B1.

These experimental results indicate a reasonable height of the masonry wall is essential to avoid splitting-tension failure under concentrated loads. Based on the minimum inclination angle of 55 degrees in specimen B2, and assuming a horizontal distance between the loading point and the nearest support equal to  $D_1$ , the height of masonry wall  $H$  needs to satisfy the condition indicated in Eq. (1).

$$H \leq D_1 \times \tan(55^\circ) \quad (1)$$

For walls with higher ratios additional structural measures such as RC tie-columns, should be installed to prevent the splitting-tension failure.

Therefore, for a SPMC wall-beam under concentrated loads, the height-to-span ratio of the masonry wall should satisfy Eq. (2) so as to cause an arch effect in the masonry wall.

$$0.25 < h_w / l_0 \leq D_1 \times \tan(55^\circ) / l_0 \quad (2)$$

In addition to the diagonal-tension and shear-compression cracks in specimen B5, several vertical compression cracks also occurred in the masonry wall. These vertical cracks are caused by axial compression, which implies that the flexural stiffness of the SPMC beam could be so large that the arching action in the masonry wall is severely weakened. According to the current Chinese Design Codes for Masonry Buildings (GB 50003-2011 2012), the height-to-span ratio of the RC beam in the wall-beam should be not less than 1/10, as a larger stiffness of the beam can improve its load-carrying capacity, shear performance of the above masonry wall and the local compression stress of the above masonry near supporting points. Nonetheless, a height-to-span ratio of the beam too high makes the vertical load distribution on the beam more even and thus weakens the arching action in the masonry wall. This is also confirmed by the lower buckling load compared to B4. Therefore, the failure mode of this masonry wall indicated the flexural stiffness of the SPMC beam, relative to the flexural stiffness of the masonry wall, was excessively high.

Based on research results on steel beam and masonry wall interaction (Smith *et al.* 1982), the stresses in both the masonry wall and the beam were highly dependent on the steel beam stiffness relative to the in-plane stiffness of the masonry wall. The wall-beam flexural stiffness ratio is

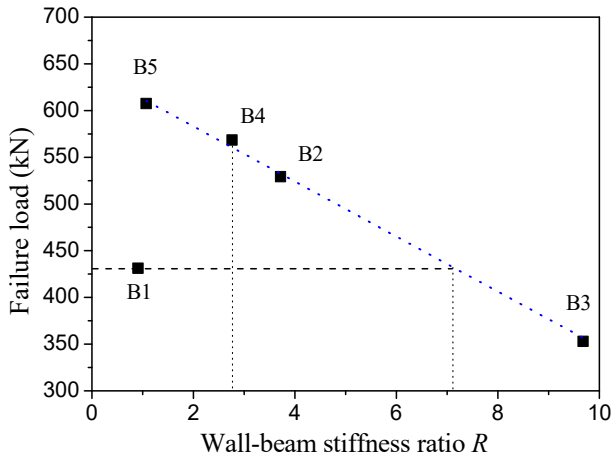


Fig. 16 Optimal arching action interval

given in Eq. (3). Where  $R$  is the ratio of the in-plane flexural stiffness of the masonry wall to the flexural stiffness of the SPMC beam;  $E_m$  is the elastic modulus (equal to  $1000f_m$ , which must not exceed 20,000 MPa (Smith *et al.* 1982),  $f_m$  is the ultimate compressive strength of masonry;  $t$  is thickness of the masonry wall;  $h_w$  is the height of the masonry wall above the SPMC beam; and  $EI$  is the flexural stiffness of the SPMC beam. A higher value of  $R$  represents a more flexible beam or a higher masonry wall, whereas a lower value of  $R$  represents a stiffer beam or a lower masonry wall.

$$R = \frac{E_m t h_w^3 / 12}{EI} = \frac{E_m t h_w^3}{12 EI} \quad (3)$$

The flexural stiffness of the SPMC beam  $EI$  is determined by Eq. (4), in which  $E_s$  is the elastic modulus of the steel plate,  $I_s$  and  $I_m$  are the second moment of area of the steel channel section and masonry beam encased by the steel channel section respectively.

$$EI = E_s I_s + E_m I_m \quad (4)$$

Based on Eqs. (3) and (4), the values of the stiffness ratio  $R$  are reported in Table 4 and are plotted in against the failure load in Fig. 16. Both the table and the plot show that the value of  $R$  affects the failure load and that there is an optimal range of values for which better development of both the arching action and interaction between masonry wall and SPMC beam is obtained.

From the previous analysis, in this experimental study the desirable failure mode of masonry wall occurred in specimens B2 and B4, which developed good arch actions and good SPMC beam-wall interaction. In specimen B3, the excessively high masonry wall led to splitting shear failure mode in the masonry wall and to a premature failure. As for specimen B5, the larger beam stiffness, compared to other specimens, although led to a higher failure load, caused the failure mode to switch to compression failure, as shown by vertical cracks in the masonry wall.

Therefore, from Table 4 a lower limit of  $R$  value for SPMC wall-beam to ensure a good beam-wall better

interaction, could be  $R = 2.76$  (specimen B4). As for the upper limit, the interval of  $R$  values of specimen B2 and B3 should be further evaluated. However, based on the linear trend of all specimens showing an arch action failure mode, it could be reasonable to exclude values of  $R$  for which the failure load falls below the failure load of B1 (which has a purely flexural behavior).

$R$  should thus verify the following inequality.

$$2.8 \leq R < 7.1 \quad (5)$$

## 5. Conclusions

This paper has presented an experiment study consisting of five SPMC beam-walls subjected to two point loads. The main conclusions drawn from the results are as follows:

- Failure of SPMC beam-walls occurred in the masonry wall for all specimens. Local buckling occurred in the side steel plates in some of the specimens before failure.
- The failure modes of the masonry walls included diagonal-tension failure, shear-compression failure, splitting-tension failure and a mixed failure with a combination of diagonal-tension, shear-compression and local compression failures.
- The main factors affecting the load-carrying capacity of a SPMC beam-wall are the thickness of the steel plates, the height-to-span ratio of the masonry wall and the wall-beam stiffness ratio.
- The arching action in the masonry wall and the interaction between the masonry wall and the SPMC beam can enhance significantly the steel local buckling load and the failure load. However, a very large height-to-span ratio of the masonry wall could reduce failure load, by causing splitting-tension failure in the masonry wall at an early stage.
- A ratio of the in-plane flexural stiffness of the masonry wall to the flexural stiffness of the SPMC beam between 2.8 to 7.1 appears to be optimal.

## Acknowledgments

The research described in this paper was financially supported by the Natural Science Foundation of Jiangsu Province, China (Grant No. BK20171361) and the National Science Foundation of China (NSFC) (Grant No. 51008070).

## References

- Borri, A., Casadei, P., Castori, G. and Hammond, J. (2009), "Strengthening of brick masonry arches with externally bonded steel reinforced composites", *ASCE J. Compos. Constr.*, **13**(6), 468-475.
- El-Diasity, M., Okail, H., Kamal, O. and Said, M. (2015), "Structural performance of confined masonry walls retrofitted using ferrocement and GFRP under in-plane cyclic loading", *Eng. Struct.*, **94**, 54-69.
- Farooq, S.H., Mohamed, A.E. and Ilyas, M. (2014a), "Seismic in-

- plane performance of retrofitted masonry walls”, *KSCE J. Civil Eng.*, **18**(1), 226-237.
- Farooq, S.H., Shahid, I. and Ilyas, M. (2014b), “Seismic performance of masonry strengthened with steel strips”, *KSCE J. Civ. Eng.*, **18**(7), 2170-2180.
- GB 50003-2011 (2012), Code for design of masonry structures; China Architecture & Building Press, Beijing, China. [In Chinese]
- GB/T 228.1-2010 (2010), Metallic materials-tensile testing-part 1: methods of test at room temperature; Standards Press of China, Beijing, China. [In Chinese]
- GB/T 50129-2011 (2011), Standard for test method of basic mechanics properties of masonry; China Architecture & Building Press, Beijing, China. [In Chinese]
- Guerreiro, J., Proença, J., Ferreira, J.G. and Gago, A. (2018), “Experimental characterization of in-plane behaviour of old masonry walls strengthened through the addition of CFRP reinforced render”, *Compos. Part B-Eng.*, **148**, 14-26.
- Hardy, S.J. (2000), “Design of steel lintels supporting masonry walls”, *Eng. Struct.*, **22**(6), 597-604.
- Hardy, S.J. and Al-Salka, M.A. (1995), “Composite action between steel lintels and masonry walls”, *Struct. Eng. Review*, **7**(2), 75-82.
- Hossain, M.M., Rahman, M.A. and All, S.S. (2000), “Parametric study of composite action between brickwall and supporting beam”, *J. Civil Eng.*, **28**(1), 51-67.
- Ismail, N., Lazzarini, D.L., Laursen, P.T. and Ingham, J.M. (2015), “Seismic performance of face loaded unreinforced masonry walls retrofitted using post-tensioning”, *Aust. J. Struct. Eng.*, **11**(3), 243-252.
- Jing, D.H. (2017), *Experimental Study and Application of Steel Plate-brick Masonry Composite Strengthening Technique*, Southeast University Press, Nanjing, Jiangsu, China. [In Chinese]
- Jing, D.H., Cao, S.Y. and Zhou, H.T. (2011), “Experimental investigation on Steel-plate-masonry composite column compressive behavior”, *Adv. Mat. Res.*, **255-260**, 591-595.
- Jing, D.H., Cao, S.Y. and Shi, L. (2012), “Flexural behaviour of steel plate-masonry composite beams”, *Steel Compos. Struct., Int. J.*, **13**(2), 123-137.
- Jing, D.H., Pan, Y.X. and Chen, Y.L. (2013), “Axial behaviour of MFT stub columns with binding bolts and epoxy adhesive”, *J. Constr. Steel Res.*, **86**, 115-127.
- Kariou, F.A., Triantafyllou, S.P., Bournas, D.A. and Koutas, L.N. (2018), “Out-of-plane response of masonry walls strengthened using textile-mortar system”, *Constr. Build. Mater.*, **165**, 769-781.
- Konthesingha, K.M.C., Masia, M.J., Petersen, R.B., Mojsilovic, N., Simundic, G. and Page, A.W. (2013), “Static cyclic in-plane shear response of damaged masonry walls retrofitted with NSM FRP strips-An experimental evaluation”, *Eng. Struct.*, **50**, 126-136.
- Martinelli, E., Perri, F., Sguazzo, C. and Faella, C. (2016), “Cyclic shear-compression tests on masonry walls strengthened with alternative configurations of CFRP strips”, *Bull. Earthquake Eng.*, **14**(6), 1695-1720.
- Preciado, A., Ramírez-Gaytan, A., Gutierrez, N., Vargas, D., Falcon, J.M. and Ochoa, G. (2018), “Nonlinear earthquake capacity of slender old masonry structures prestressed with steel, FRP and NiTi SMA tendons”, *Steel Compos. Struct., Int. J.*, **26**(2), 213-226.
- Santis, S.D., Casadei, P., Canio, G.D., Felice, G.D., Malena, M., Mongelli, M. and Roselli, I. (2016), “Seismic performance of masonry walls retrofitted with steel reinforced grout”, *Earthq. Eng. Struct. D.*, **45**(2), 229-251.
- Santis, S.D., Roscini, F. and Felice, G. (2018), “Full-scale tests on masonry vaults strengthened with steel reinforced grout”, *Compos. Part B-Eng.*, **141**, 20-36.
- Smith, B.S., Pradolin, L. and Riddington, J.R. (1982), “Composite design method for masonry walls on steel beams”, *Can. J. Civil Eng.*, **9**(1), 96-106.
- Soltis, L.A. and Tuan, Y.B. (1980), “Steel supported masonry walls”, *Eng. J.*, **17**(1), 11-13.
- Taghdi, M., Bruneau, M. and Saatcioglu, M. (2000), “Seismic retrofitting of low-rise masonry and concrete walls using steel strips”, *ASCE J. Struct. Eng.*, **126**(9), 1017-1025.
- Wang, X., Lam, C.C. and Iu, V.P. (2018), “Experimental investigation of in-plane shear behaviour of grey clay brick masonry panels strengthened with SRG”, *Eng. Struct.*, **162**, 84-96.

BU